Available online at www.sciencedirect.com
ScienceDirect
Journal of Power Sources 177 (2008) 624–630
JOURNAL OF POWER SOURCES
www.elsevier.com/locate/jpowsour

# Electrochemical behavior of Mg–Li, Mg–Li–Al and Mg–Li–Al–Ce in sodium chloride solution

Dianxue Cao *, Lin Wu, Yong Sun, Guiling Wang, Yanzhuo Lv

*Key Laboratory of Superlight Material and Surface Technology of Ministry of Education, College of Material Science and Chemical Engineering, Harbin Engineering University, Harbin 150001, PR China*

Received 11 October 2007; received in revised form 13 November 2007; accepted 13 November 2007
Available online 21 November 2007

**Abstract**

Mg–Li, Mg–Li–Al and Mg–Li–Al–Ce alloys were prepared and their electrochemical behavior in 0.7 M NaCl solutions was investigated by means of potentiodynamic polarization, potentiostatic current–time and electrochemical impedance spectroscopy measurements as well as by scanning electron microscopy examination. The effect of gallium oxide as an electrolyte additive on the potentiostatic discharge performance of these magnesium alloys was studied. The discharge activities and utilization efficiencies of these alloys increase in the order: Mg–Li < Mg–Li–Al < Mg–Li–Al–Ce, both in the absence and presence of $Ga_2O_3$. These alloys are more active than commercial magnesium alloy AZ31. The addition of $Ga_2O_3$ into NaCl electrolyte solution improved the discharging currents of the alloys by more than 4%, and enhanced the utilization efficiencies of the alloys by more than 6%. It also shortened the transition time for the discharge current to reach to a steady value. Electrochemical impedance spectroscopy measurements showed that the polarization resistance of the alloys decreases in the following order: Mg–Li > Mg–Li–Al > Mg–Li–Al–Ce. Mg–Li–Al–Ce exhibited the best performance in term of activity, utilization efficiency and activation time.


*Keywords:* Mg–Li; Mg–Li–Al; Mg–Li–Al–Ce; $Ga_2O_3$; Electrochemical performance; Utilization efficiency

## 1. Introduction

Metal-hydrogen peroxide semi fuel cells have been studied as power sources for unmanned underwater vehicles (UUV) because of their high specific energy, stable discharging ability, short mechanically recharge time, long dry storage life, ability to work at ambient pressure, environment acceptability, reliability, safety and low cost [1–8]. Aluminum and magnesium are attractive anode materials for this type of semi fuel cell because aluminum and magnesium have high Faradic capacity (Al: 2.98 Ah $g^{-1}$, Mg: 2.2 Ah $g^{-1}$), high specific energy (Al: 8.1 kW h $g^{-1}$, Mg: 6.8 kW h $kg^{-1}$), more negative standard electroreduction potentials versus standard hydrogen electrode (Al: −2.31 V in alkaline solution, Mg: −2.37 V in neutral solution) [9]. An Al–$H_2O_2$ semi fuel cell stack, composed of six serially connected cells with circulating 7 M KOH as electrolyte, developed by Hasvold et al., has an energy content of up to 50 kW h per refill of electrolyte and an energy density of 100 W h $kg^{-1}$ based on total system weight (472 kg). This power system gives an UUV of 1400 kg dry weight an endurance of typically 60 h at 4 knots at a maximum operation depth of 3000 m [2,10]. Mg–$H_2O_2$ semi fuel cells investigated by Medeiros et al. use magnesium alloy AZ61 as anode, carbon fiber supported Pd–Ir as cathode catalyst, $H_2O_2 + H_2SO_4$ as cathode active components, seawater as electrolyte, and Nafion-115 as membrane. The cell has a theoretical voltage of 4.14 V. The practical cell voltage is above 1.7 V at 25 mA $cm^{-2}$ with magnesium and hydrogen peroxide efficiencies ranging from 77 to 86%, and specific energies ranging from 500 to 520 W h $kg^{-1}$ based on the weights consumed during discharge of the magnesium anode, hydrogen peroxide and acid [1,11,12].

Thermodynamically aluminum and magnesium anodes should exhibit very negative potentials. However, in practical, these electrodes operate at significantly less negative potentials because (a) aluminum and magnesium are normally covered by passive oxide films which cause a delay in reaching a

* Corresponding author. Tel.: +86 451 82589036; fax: +86 451 82589036.
*E-mail address:* caodianxue@hrbeu.edu.cn (D. Cao).

0378-7753/$ – see front matter © 2007 Elsevier B.V. All rights reserved.
doi:10.1016/j.jpowsour.2007.11.037

steady-state and reduce discharging rate; (b) aluminum and magnesium undergo parasitic corrosion reactions, or self-discharge, resulting in the reduction of Columbic efficiency (less than 100% utilization of the metal) and the evolution of hydrogen. There are in general two ways to improve the anode performance. One is to dope the aluminum or magnesium with other elements (known as "activation"). The second is to modify the electrolyte by including additives. Both methods can inhabit the formation and/or accelerate the elimination of oxide layers and suppress corrosive dissolution [13].

The enhancement of aluminum anode performance by adding alloying elements to pure aluminum or by adding additives to electrolytes has been widely studied. For example, the incorporation of small concentrations of metals such as magnesium, calcium, zinc, gallium, indium, thallium, and lead, usually in combinations as ternary or quaternary alloys, has been found to be effective in improving discharging current and inhibition of corrosion [14,15]. Oxides of gallium, indium, calcium and zinc as well as stannates and citrates were found to be effective electrolyte additives for inhibiting corrosion and/or boosting the electrode potential [16–19]. However, the improvement of magnesium anode performance by the addition of alloying elements to pure magnesium and the use of additives in electrolytes has not been well investigated [20,21]. Udhayan et al. reported that magnesium alloy AP65 (Al: 6–7%, Pb: 4.5–5%, Zn: 0.14–1.5%, Mn: 0.15–1.3%) has a hydrogen evolution rate of 0.15 mL $min^{-1}$ $cm^{-2}$ and a utilization efficiency of 84.6%. The open circuit potential of this alloy is −1.803 V(vs. SCE) measured in seawater [20]. Sivashanmugam et al. investigated Mg–Li alloy with 13 wt.% Li for possible use in magnesium primary reserve batteries [22]. They found that this Mg–Li alloy exhibits higher anodic efficiencies (81%) even when the current density is increased to 8.6 mA $cm^{-2}$. The Mg–Li/$MgCl_2$/CuO cells offer higher operating voltage and capacity than those with the conventionally used Mg–Al alloy. Comparing to the aluminium–$H_2O_2$ semi fuel cell with strong alkaline (NaOH or KOH) as electrolytes, magnesium–$H_2O_2$ semi fuel cell uses seawater as electrolytes and it has higher theoretical voltage, which make it more attractive as undersea power sources.

In this study, binary Mg–Li, ternary Mg–Li–Al and quaternary Mg–Li–Al–Ce alloys were prepared. Their discharge performance in NaCl solution (the electrolyte for Mg–$H_2O_2$ semi fuel cell and magnesium seawater battery) was studied. The effect of the addition of gallium oxide to NaCl solution on the activation and self-discharge of these magnesium alloy anodes was examined.

## 2. Experimental

### 2.1. Preparation of magnesium alloys

Mg–Li, Mg–Li–Al and Mg–Li–Al–Ce alloys were prepared from ingots of pure magnesium (99.99%), pure lithium (99.99%), pure aluminum (99.99%) and Mg–Ce alloy containing 26.6 wt.% Ce using a vacuum induction melting furnace. The induction furnace containing a refractory lined crucible surrounded by an induction coil is located inside a vacuum chamber.

Table 1
Nominal composition of the alloys (wt.%)

| Alloys | Mg | Li | Al | Ce |
|---|---|---|---|---|
| Mg–Li | 92 | 8 | – | – |
| Mg–Li–Al | 89 | 8 | 3 | – |
| Mg–Li–Al–Ce | 88 | 8 | 3 | 1 |

The induction furnace is connected to an AC power source at a frequency precisely matched to the furnace size and material being melted. Magnesium and the alloying components were charged into the induction furnace under the protection of ultrahigh purity argon, the furnace was then evacuated to $1.0 \times 10^{-2}$ Pa, and charged with ultrahigh purity argon. AC power was applied to melt the charge under flowing argon atmosphere. A preheated tundish-casting mold assembly was inserted through a valve, and the refractory tundish was positioned in front of the induction furnace. The molten metals were poured through the tundish into the awaiting stainless steel mold ($\phi$6 cm × 18 cm). The mold containing hot melts was cooled down to ambient temperature under argon atmosphere in the furnace within 2 h. The prepared alloys were used in the cast state. The compositions of the alloys are given in Table 1.

The alloy ingots were machined to 20 mm × 20 mm × 2 mm to serve as the working electrode for electrochemical measurements. Prior to each experiment, the alloy surface facing to the electrolyte was mechanically polished with SiC abrasive paper down to 700 grit, degreased with acetone, washed with deoxygenated ultrapure water (Milli-Q), and then immediately assembled into the electrochemical cell.

### 2.2. Electrochemical measurements

A three-electrode electrochemical cell was made of Pyrex glass and Teflon (Fig. 1). The cell was fitted with a blackened platinum gauze auxiliary electrode and a saturated calomel reference electrode (SCE) with the Luggin capillary positioned

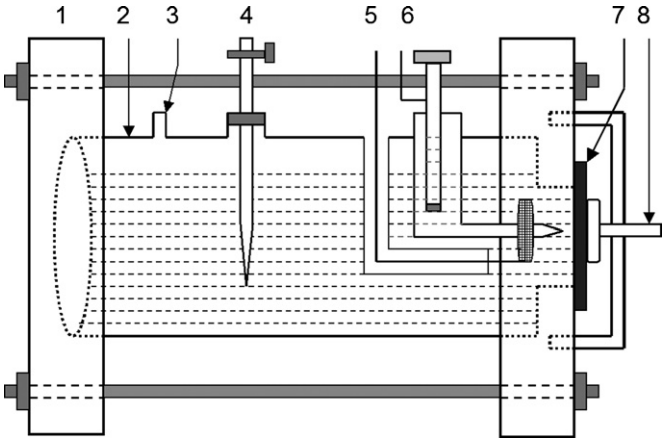


Fig. 1. The descriptive diagram of the three-electrode electrochemical cell with defined exposure area for working electrode. (1) Teflon end block; (2) cylindric glass cell body; (3) inert gas outlet; (4) inert gas inlet; (5) counter electrode; (6) reference electrode and Luggin capillary; (7) working electrode (alloy slice); (8) screw for fastening working electrode.

closing to the alloy surface. The exposure area of the metal alloy electrode is 0.95 $cm^2$, which was used to calculate the current density. Electrochemical experiments were carried out at room temperature in 0.7 M NaCl aqueous solutions (purged with Ar before transferred into the cell), chosen in order to mimic seawater. All solutions were made with analytical grade chemical reagents and Millipore Milli-Q water (resistivity >18 MΩ cm). The measurements of potentiodynamic polarization curves (5 mV $s^{-1}$, −2.2 to −0.8 V vs. SCE), potentiostatic current–time curves (−1.0 V vs. SCE), and electrochemical impedance spectra (1 to 200,000 Hz, open circuit potential) were performed using an eight channel VMP3/Z potentiostat (Princeton Applied Research) controlled by EC-lab software. The morphology of the alloy surface was examined using scanning electron microscopy (SEM; JEOL JSM-6480) equipped with energy dispersive spectroscopy (EDS unit). Images were acquired using a 20 kV accelerating voltage.

In order to measure the utilization efficiency of the metal alloys, the weighted alloy coupons were discharged at −1.0 V for 60 min while recording the current–time curves. The reaction products remaining attached on the alloy surfaces after discharge were removed using a scratch blade and high speed water spray. The cleaned remaining alloy coupons were then dried and weighed. The alloy utilization efficiency ($\eta$) was calculated using Eq. (1).

$$\eta = \frac{(Q/nF)M_a}{W_i - W_f} \times 100\% \quad (1)$$

where $Q$ is the charge in Coulomb obtained by the integration of current–time curve, $F$ is Faraday constant (96485 C $mol^{-1}$), $W_i$ and $W_f$ are the weight of alloy sample in gram before and after discharge, respectively, $n$ is the average number of electron per discharge reaction assuming the oxidation states of the products are 2+ for Mg, 1+ for Li, 3+ for Al and Ce. $M_a$ is the average atomic mass (g $mol^{-1}$) of the sample. $n$ and $M_a$ were calculated by Eqs. (2) and (3), respectively.

$$n = \sum x_i z_i \quad (2)$$

$$M_a = \sum x_i M_i \quad (3)$$

where $x_i$ is the mole fraction, $z_i$ is the oxidation state, and $M_i$ is the atomic mass of component $i$.

## 3. Results and discussions

### 3.1. Potentiodynamic polarization

Fig. 2 shows the potentiodynamic polarization curves of Mg–Li, Mg–Li–Al and Mg–Li–Al–Ce measured in 0.7 M NaCl solution (1st sweep in the positive-going direction). The curves were taken after the electrodes were cathodically polarized at −2.2 V vs. SCE for 2 min. The curves of pure Mg and commercial magnesium–aluminum alloy AZ31 (Al: 3.5%, Zn: 1.2%) were also measured and included in the figure for comparison. The curve of pure Mg is in good agreement with that reported in literatures [23,24]. The corrosion potential of Mg–Li (−1.67 V) is slightly more negative than that of pure Mg (−1.63 V), and the anodic current of Mg–Li near the corrosion potential region is higher than that of pure Mg, implying that Mg–Li is less corrosion resistant than pure Mg, which might be attributed to the high activity of Li. The corrosion potential of Mg–Li–Al is −1.47 V, which is 200 mV more positive than that of Mg–Li, and is close to that of AZ31 (−1.45 V), indicating that the presence of Al as an alloying element obviously enhanced the corrosion inhibition ability of Mg–Li alloy. The corrosion potential of Mg–Li–Al–Ce is −1.53 V, around 100 mV more negative than that of Mg–Li–Al, demonstrating that the addition of Ce decreased the corrosion resistivity of Mg–Li–Al. For all the samples, there are passive regions in their anodic polarization curves corresponding to the formation of anodic film. The anodic films act as physical shields between metal and medium to prohibit the alloys from self-discharge. The anodic curve of Mg–Li–Al–Ce differs from other alloys with lager overpotential for reaching its passivation region, an indication of a different self-discharge behavior.

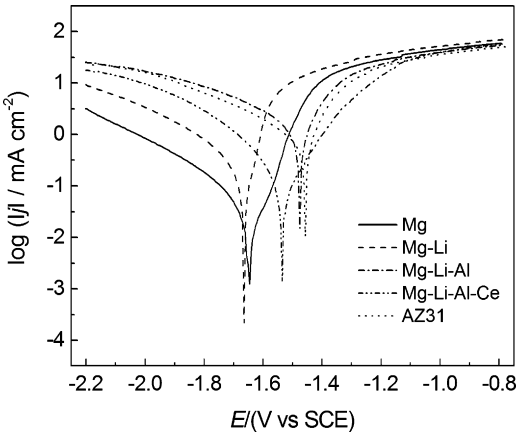


Fig. 2. Potentiodynamic polarization curves for Mg–Li, Mg–Li–Al, Mg–Li–Al–Ce, Mg and AZ31 measured in 0.7 M NaCl solution at a scan rate of 5 mV $s^{-1}$.

### 3.2. Potentiostatic measurements

The current–time curves measured at −1.0 V in 0.7 M NaCl are shown in Fig. 3. The potential was chosen to be in the passive region for all the samples. The current–time profiles are similar for all the samples, i.e. the anodic current increased rapidly in the early discharging stage and then reached to an approximate constant value. Among all the samples, Mg–Li–Al–Ce displays the highest anodic current density of 44 mA $cm^{-2}$, around 3 mA $cm^{-2}$ higher than pure Mg, Mg–Li and Mg–Li–Al, 10 mA $cm^{-2}$ higher than commercial AZ31. Looking closely at the initial discharge period, it can be seen that it took shorter time for current to reach to the steady value for Mg–Li–Al–Ce than for other samples, which means that Mg–Li–Al–Ce gives shorter activation time and thereby shorter voltage transience on switching between loads. This property is important for serving as anode in fuel cells or batteries needing a short period of high discharge. The potentiostatic current–time measurements lead to the conclusion that quaternary Mg–Li–Al–Ce is more

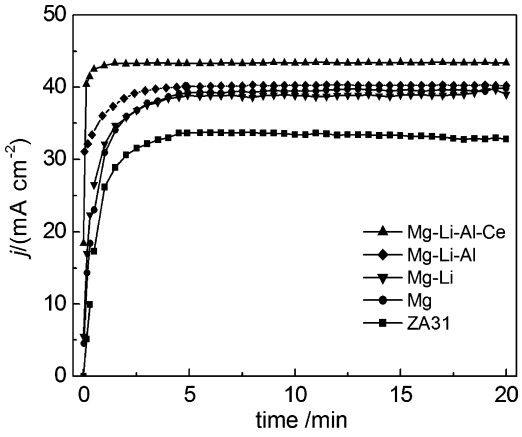


Fig. 3. Current–time curves for Mg–Li, Mg–Li–Al, Mg–Li–Al–Ce, Mg and AZ31 recorded in 0.7 M NaCl solution at a constant potential of −1.0 V.

active than ternary Mg–Li–Al and binary Mg–Li alloy, and Mg–Li-based alloys show better discharge performance than commercial magnesium–aluminum alloy AZ31 under the same experimental condition. The discharging current densities of our prepared Mg–Li based alloys are higher than aluminum alloys under the similar experimental condition. For example, the current density of Al–In and Al–In–Ga polarized at −1.05 V vs. SCE for 20 min in 0.6 M NaCl are around 32 mA cm$^{-2}$ and 7.5 mA cm$^{-2}$, respectively [25]. It should be noted that the discharge currents for all the three Mg–Li based alloys display no sign of decrease within 20 min test period.

Fig. 4a–c shows the SEM micrographs of AZ31 (a), Mg–Li (b), Mg–Li–Al (c) and Mg–Li–Al–Ce (d), taken after discharge at −1.0 V for 20 min in 0.7 M NaCl. Fig. 4a indicated that the oxidation products of AZ31 formed thick and large micro-blocks on the surface. Fig. 4b and d demonstrated that the discharge products remaining attached on Mg–Li, Mg–Li–Al and Mg–Li–Al–Ce surface present as loosely packed aggregates of particles. Obviously, the discharge products of the four alloys existed in different forms on the surfaces. The loosely packed oxidation products of three Mg–Li alloys allowed the electrolyte to penetrate through, besides, they peeled off more easily. As a result, Mg–Li based alloy retain large reaction surface during discharge, which in turn enabled the high discharging currents.

The complex impedance technique was used as a basis for a comparative study to show the discharge behavior of the alloys. The electrochemical impedance spectroscopies of Mg–Li, Mg–Li–Al and Mg–Li–Al–Ce, as well as pure Mg and commercial AZ31 were recorded at open circuit potential in 0.7 M NaCl solution. The measurements were performed immediately after the samples were discharged at −1.0 V for 20 min in order to obtain steady state conditions. The Nyquist plots are shown in Fig. 5. A single capacitive semicircle was observed for all the samples tested. The diameter, representing the polarization resistance $R_p$, for Mg–Li–Al–Ce (ca. 4 Ω cm$^2$) and for Mg–Li–Al (ca.7 Ω cm$^2$) is smaller than that for Mg–Li (ca.

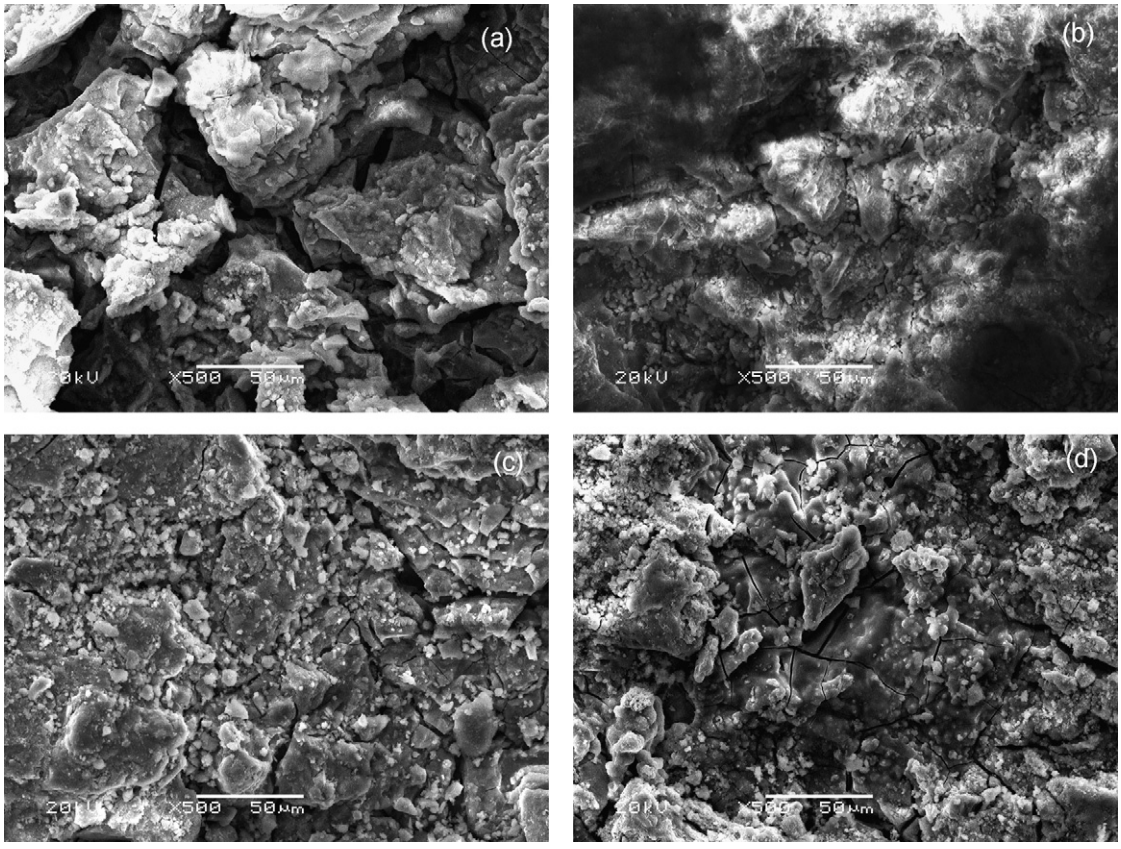


Fig. 4. SEM micrographs of (a) AZ31, (b) Mg–Li, (c) Mg–Li–Al and (d) M–Li–Al–Ce obtained after potentiostatic discharge at −1.0 V for 20 min in 0.7 M NaCl solution.

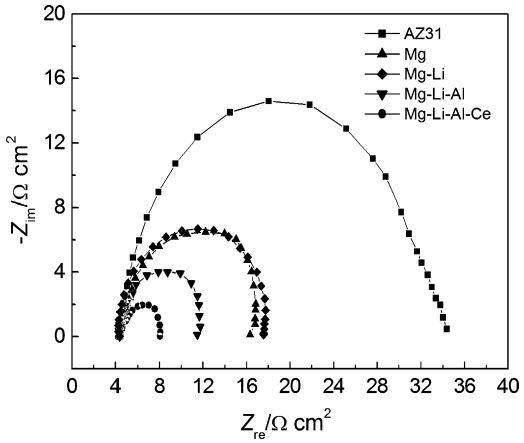


Fig. 5. Impedance spectra for Mg–Li, Mg–Li–Al, Mg–Li–Al–Ce, Mg and AZ31 recorded at open circuit potential in 0.7 M NaCl after discharge at −1.0 V for 20 min in 0.7 M NaCl.

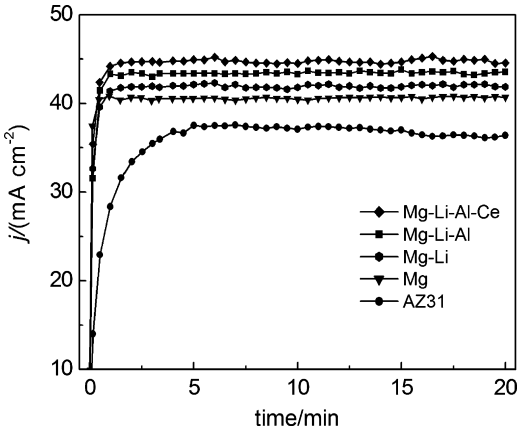


Fig. 6. Current–time curves measured at −1.0 V for Mg–Li, Mg–Li–Al, Mg–Li–Al–Ce, Mg and AZ31 in 0.7 M NaCl containing 0.05 mM $Ga_2O_3$.

13.5 Ω cm$^2$). Mg–Li and pure Mg displayed a similar polarization resistance. All the Mg–Li based alloys show much smaller polarization resistance than AZ31 (ca. 30 Ω cm$^2$). The alloys can be arranged according to the increase in the polarization resistance, as determined from the capacitive loop, in the order: AZ31 > Mg ≈ Mg–Li > Mg–Li–Al > Mg–Li–Al–Ce. This indicates that Mg–Li–Al–Ce alloy presents the most active behavior compared with other alloys, which is in agreement with the above-mentioned results of current–time measurements. Song et al. reported that the EIS of magnesium anodic polarized at 90 mV higher than corrosion potential in 1 M NaCl displayed two loops, an inductive loop in the middle frequency range, and a capacitive loop in the low frequency region. The inductive loop was attributed to the broken area of the protective surface film [24]. The inductive loop was not observed, however, in this study. This is probably because the high anodic polarization potential applied during discharge (630 mV more positive than corrosion potential) results in the absence of surface film. The same arguments might be applicable to other magnesium alloys tested. The EIS spectrum of AZ31 is in good agreement with that reported by Udhayan and Bhatt [26] recorded in 2.0 M magnesium perchlorate solution.

### *3.3. Effects of electrolyte additive $Ga_2O_3$ on discharge performance*

Electrolyte additives can effectively enhance the discharge performance of metal anodes. For example, dithiobiuret, stannate and quaternary ammonium salt have been reported to be effective additives for magnesium anode. The anode utilization efficiency of AZ31 alloy was increased by 13% to reach 90% by using a combination additive of quaternary ammonium salt Aliquat 336 and stannate [21]. In this study, gallium oxide was investigated as electrolyte additive for Mg–Li based alloy anodes. Fig. 6 shows the current–time curves recorded at −1.0 V in 0.7 M NaCl containing 0.05 mM $Ga_2O_3$. In comparison with Fig. 3, it can be seen that the presence of $Ga_2O_3$ in NaCl electrolyte improved the discharge current densities of all the samples. Around 10% increase in current density was observed for AZ31, around 7% for Mg–Li and Mg–Li–Al, and approximate 4% for Mg–Li–Al–Ce and pure Mg. Interestingly, the presence of $Ga_2O_3$ in NaCl electrolyte also shortened the transition time for potentiostatic discharge currents of Mg–Li, Mg–Li–Al and pure Mg reaching to constant values.

The surface morphologies of AZ31, Mg–Li, Mg–Li–Al and Mg–Li–Al–Ce after discharge at −1.0 V for 20 min in $Ga_2O_3$ containing NaCl solution were examined by SEM. The images are given in Fig. 7. By comparing Fig. 7a–d with Fig. 4a–d, it was found that the addition of $Ga_2O_3$ to the electrolyte markedly changed the morphology of the oxidized surfaces of all the alloys tested. For AZ31 the size and thickness of the micro-clumps of oxidation products formed during discharge became smaller. For Mg–Li the product particles became finer and loosely packed. For Mg–Li–Al and Mg–Li–Al–Ce, the products packed by layers perpendicular to the surface. This pattern significantly differs from that in the absence of $Ga_2O_3$. Some needle crystals were formed on the Mg–Li–Al–Ce surface. These observations suggested that $Ga_2O_3$ acted as an active additive to loosen the product film and promote the coming off the shedding of oxidation products, consequently enhancing the discharge performance of all the magnesium alloys.

The anode utilization efficiencies of Mg–Li, Mg–Li–Al and Mg–Li–Al–Ce, as well as pure Mg and AZ31 were measured using a weight loss method. The measurements were carried out after discharging the samples at −1.0 V for 60 min in 0.7 M NaCl solution with and without $Ga_2O_3$. The utilization efficiency is defined as the percentage of the mass loss responsible for the generation of discharge current to the total mass loss within the discharge period. The results are given in Table 2. In the absence of $Ga_2O_3$, the utilization efficiency of Mg–Li–Al–Ce is around 82%, higher than AZ31 (75%), but slightly lower than the state-of-the-art magnesium alloy anode, AP65 (84.7%) [20]. The utilization efficiency of the three Mg–Li based alloys increases in the order: binary < ternary < quaternary. Pure magnesium has the lowest utilization efficiency. These results indicated that the utilization efficiency of magnesium can be enhanced significantly by alloying with Li, Al and Ce. As it is well known that alloying, on one hand, reduces crystal grain size, resulting in an increase of hydrogen evolution overpotential and a decrease of

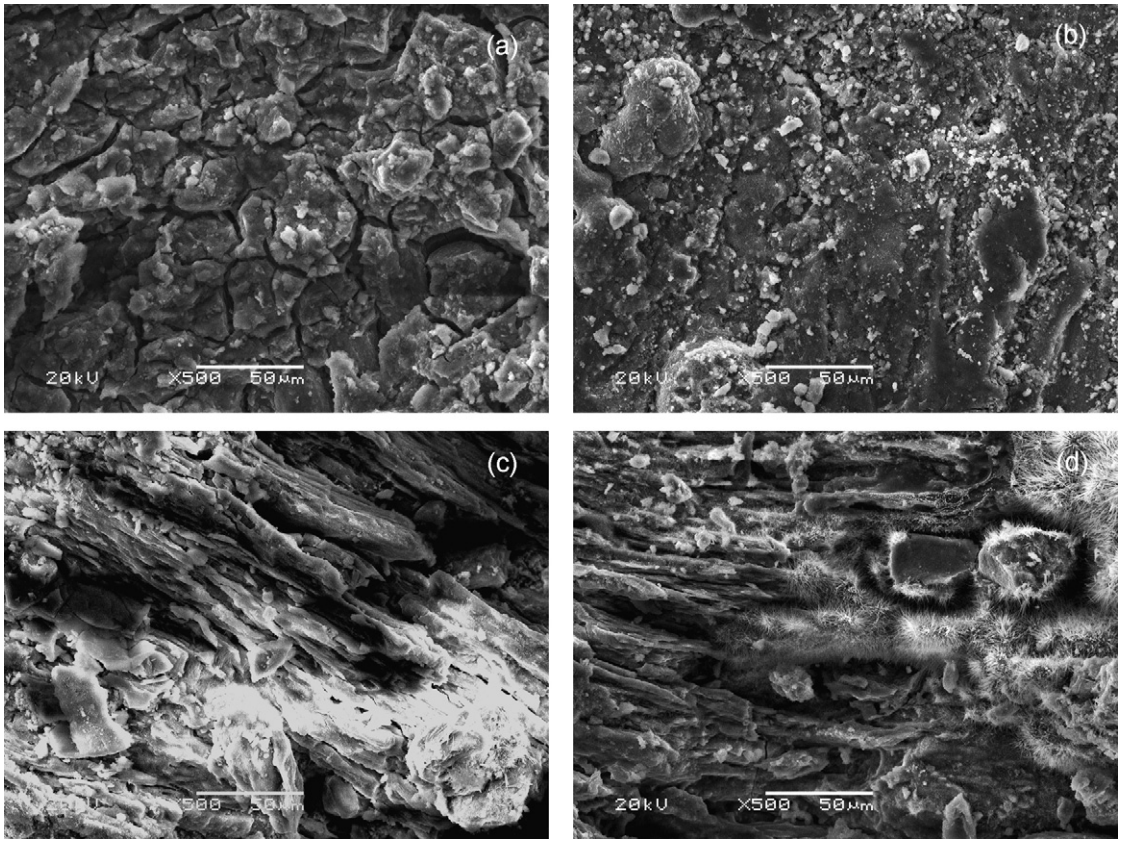


Fig. 7. SEM micrographs of (a) AZ31, (b) Mg–Li, (c) Mg–Li–Al and (d) Mg–Li–Al–Ce obtained after potentiostatic discharge at −1.0 V for 20 min in 0.7 M NaCl containing 0.05 mM $Ga_2O_3$.

Table 2
Utilization efficiencies of alloys in the absence and presence of gallium oxide

| | Utilization efficiency $\eta$ (%) | | | | |
|---|---|---|---|---|---|
| | Mg–Li | Mg–Li–Al | Mg–Li–Al–Ce | Mg | AZ31 |
| 0.7 M NaCl | 68.8 | 76.6 | 81.8 | 54.4 | 75.2 |
| 0.7 M NaCl + 0.05 mM $Ga_2O_3$ | 76.9 | 84.4 | 87.6 | 62.1 | 83.3 |

self-discharge rate, on the other hand, prevents the formation of passive coatings on the surface or destroys the dense structure of surface films to facilitate their peeling off from alloy surfaces, either way leading to an enhancement of discharge performance.

The addition of 0.05 mM $Ga_2O_3$ to NaCl solution improved the utilization efficiencies by around 8% for Mg–Li, Mg–Li–Al, Mg and AZ31, and 6% for Mg–Li–Al–Ce. The utilization efficiency of Mg–Li–Al–Ce in 0.7 M NaCl containing 0.05 mM $Ga_2O_3$ reached to as high as 87.6%. Clearly, $Ga_2O_3$ is an effective electrolyte additive for reducing mass loss of magnesium alloys caused by corrosion and other parasitic reactions.

## 4. Conclusions

Casting ingots of Mg–Li, Mg–Li–Al and Mg–Li–Al–Ce alloys were prepared by induction smelting the pure metals with each other or with a Mg–Ce alloy under Ar atmosphere followed by surface grinding and cleaning. Their properties as potential anode material for metal semi fuel cell and seawater battery were investigated and compared with pure magnesium and commercial magnesium alloy AZ31. These three Mg–Li based alloys demonstrated higher potentiostatic discharge current in NaCl solution than AZ31. The oxidation products of Mg–Li, Mg–Li–Al and Mg–Li–Al–Ce were loosely adhered to the alloys surfaces, which is partially responsible for the high discharge activity. Gallium oxide electrolyte additive enhanced that discharge currents and utilization efficiencies of the three alloys prepared. The utilization efficiency of the quaternary Mg–Li–Al–Ce reaches to as high as around 82% and 88% in the absence and presence of gallium oxide additive, respectively. The transition time for discharge current to reach to steady state was shortened by the addition of gallium oxide.

## Acknowledgements

We gratefully acknowledge to Dr. Milin Zhang for assistance in alloy preparation. This work was financially supported by Key Laboratory of Superlight Material and Surface Tech-

nology of Ministry of Education and Harbin Engineering University.

## References

[1] M.G. Medeiros, R.R. Bessette, C.M. Deschenes, C.J. Patrissi, L.G. Carreiro, S.P. Tucker, D.W. Atwater, J. Power Sources 136 (2004) 226–231.
[2] O. Hasvold, N.J. Storkersen, S. Forseth, T. Lian, J. Power Sources 162 (2006) 935.
[3] W. Yang, S. Yang, W. Sun, G. Sun, Q. Xin, J. Power Sources 160 (2006) 1420.
[4] W. Yang, S. Yang, W. Sun, G. Sun, Q. Xin, Electrochim. Acta 52 (2006) 9.
[5] D.J. Brodrecht, J.J. Rusek, Appl. Energ. 74 (2003) 113–124.
[6] R.R. Bessette, M.G. Medeiros, C.J. Patrissi, C.M. Deschenes, C.N. LaFratta, J. Power Sources 96 (2001) 240–244.
[7] R.R. Bessette, J.M. Cichon, D.W. Dischert, E.G. Dow, J. Power Sources 80 (1999) 248–253.
[8] M.G. Medeiros, C.G. Zoski, J. Phy. Chem. B 102 (1998) 9908–9914.
[9] R.P. Hamlen, D.W. Atwater, in: D. Linden, T.B. Reddy (Eds.), Handbook of Batteries, third ed., McGraw-Hill, 2002, p. 381.
[10] O. Hasvold, N. Storkersen, J. Power Sources 96 (2001) 252–258.
[11] M.G. Medeiros, R.R. Bessette, C.M. Deschenes, D.W. Atwater, J. Power Sources 96 (2001) 236–239.
[12] M.G. Medeiros, E.G. Dow, J. Power Sources 80 (1999) 78–82.
[13] Q. Li, N.J. Bjerrum, J. Power Sources 110 (2002) 1.
[14] T. Valand, G. Nilsson, Corros. Sci. 17 (1977) 931.
[15] A. Mance, D. Cerovic, A. Mihajlovic, J. Appl. Electrochem. 14 (1984) 459.
[16] I.J. Albert, M.A. Kulandainathan, M. Ganesan, V. Kapali, J. Appl. Electrochem. 19 (1989) 547.
[17] M.L. Doche, F. Novel-Cattin, R. Durand, J.J. Rameau, J. Power Sources 65 (1997) 197–205.
[18] V. Kapali, S.V. Iyer, V. Balaramachandran, K.B. Sarangapani, M. Ganesan, M.A. Kulandainathan, A. Sheik Mideen, J. Power Sources 39 (1992) 263–269.
[19] K.B. Sarangapani, V. Balaramachandran, V. Kapali, S.V. Iyer, M.G. Potdar, K.S. Rajagopalan, J. Appl. Electrochem. 14 (1984) 475–480.
[20] R. Udhayan, N. Muniyandi, P.B. Mathur, Br. Corros. J. 27 (1992) 68–71.
[21] K.H. Oehr, S. Splinter, J.C.-Y. Jung, E.L. Gyenge, C.W. Oloman, US 6,706,432 (2004).
[22] A. Sivashanmugam, T.P. kumar, N.G. Renganathan, S. Gopukumar1, J. Appl. Electrochem. 34 (2004) 1135–1139.
[23] G. Song, A. Atrens, D. Stjohn, J. Nairn, Y. Li, Corros. Sci. 39 (1997) 855–875.
[24] G. Song, A. Atrens, D.S. John, X. Wu, J. Nairn, Corros. Sci. 39 (1997) 1981–2004.
[25] H.A. El Shayeb, F.M. Abd El Wahab, S. Zein El Abedin, Corros. Sci. 43 (2001) 643.
[26] R. Udhayan, D.P. Bhatt, J. Power Sources 63 (1996) 103.